

Thrombin-Loaded Magnetic Microbubbles for the Treatment of Pseudoaneurysms

Alec Thomas, Bernard Shieh, Luca Bau, Regent Lee, Ashok Handa, and Eleanor Stride*

The drive toward minimally invasive surgery has yielded multiple benefits for patients but has also increased the incidence of pseudoaneurysms (PSA). The current standard of care is ultrasound-guided thrombin injection to coagulate blood in the PSA sac and seal the ruptured vessel. There is, however, a risk of downstream thrombosis if thrombin escapes into the communicating vessel and this limits patient eligibility for thrombin injection. In this study, the feasibility of using magnetic targeting to reduce the risk of distal thrombosis is investigated. Thrombin-loaded magnetic microbubbles are formulated and injected into tissue-mimicking phantoms of PSAs with different geometries using either saline or whole (equine) blood. Ultrasound imaging is used to quantify the concentration of bubbles remaining in the sac with and without application of a custom-built magnetic array. An absorbance-based assay is also used to quantify the concentration of thrombin escaping from the sac. Magnetic targeting enables a significant increase in thrombin retention in all femoral artery PSA models except one, with up to $97\% \pm 2.5\%$ of the injected thrombin being retained. It is also confirmed that the enzymatic activity of thrombin is maintained, and that clot formation can be successfully achieved in whole blood.

patients that are on both antiplatelet and anticoagulation therapy have a higher likelihood of vascular complications. Though few deaths are attributed to PSAs, they impose a large burden upon patients and health-care providers due to distal embolization, infection, compression on nearby vasculature and/or nerves and the corresponding increase in length of hospital stays.^[2]

PSAs result from the removal of a catheter and the inability of the perforation site to seal. The puncture allows blood to continuously perfuse into the perivascular space, at arterial pressure, forming a sac that is surrounded by either adventitia or soft tissue and communicates with the main vessel through the PSA neck (Figure 1). The anatomy of a PSA can vary greatly from patient to patient with neck lengths and diameters from 2 to 10 mm and from 2 to 8 mm, respectively, and sac diameters from 10 to 50 mm.^[3] The most

significant complication is rupture of the sac resulting in severe hemorrhaging. Therefore, for symptomatic patients, it is desirable to treat the condition as quickly as possible.

Up until the early 2000s, ultrasound-guided compression therapy was used widely to arrest blood flow and induce coagulation of the PSA sac.^[3b,4] However, due to treatment times of up to an hour, significant discomfort to the patient, high failure rates (up to 70%), and compression induced ischemia to the surrounding tissue causing subcutaneous necrosis, this technique was supplanted by ultrasound-guided thrombin injection (UGTI).^[4,5] For qualifying patients, UGTI is highly effective with a success rate of about 88% because thrombin rapidly (within seconds) coagulates blood and creates a hemostatic plug at the puncture site.^[5d,6]

Thrombin (Factor IIa) is the key enzyme in the blood coagulation pathway that converts fibrinogen into insoluble fibrin by selectively cleaving the Arg–Gly bonds. Thrombin also activates cofactors (Factors VIII, V, and IX) to stimulate crosslinking of fibrin in the presence of calcium.^[5d] Moreover, thrombin facilitates platelet recruitment and attachment to the clot, which is critical in forming hemostatic plugs and promoting wound healing. Thrombin has been used clinically for over 50 years as an intraoperative surgical glue.^[5e,f] For example, Tisseel (Baxter, USA) is a fibrin sealant that contains two separated components, fibrinogen and thrombin. These components are mixed as they are applied to the affected area creating a biocompatible seal. However, frequently the kit is used off-label for UGTI and half

1. Introduction

Femoral artery pseudoaneurysms (PSAs) occur in over 400 000 patients worldwide annually, making them the most prevalent complication during interventional femoral artery access.^[1] The popularity of minimally invasive procedures for diagnostic and interventional purposes is on the rise (>7 million annually) and

A. Thomas, B. Shieh, L. Bau, E. Stride
Institute of Biomedical Engineering
Department of Engineering Sciences
Old Road Campus Research Building
University of Oxford
Headington, Oxford OX3 7DQ, UK
E-mail: eleanor.stride@eng.ox.ac.uk

R. Lee, A. Handa
Nuffield Department of Surgical Sciences
Room 6607
Level 6 John Radcliffe Hospital
University of Oxford
Oxford OX3 9DU, UK

© 2022 The Authors. Advanced Therapeutics published by Wiley-VCH GmbH. This is an open access article under the terms of the Creative Commons Attribution License, which permits use, distribution and reproduction in any medium, provided the original work is properly cited.

DOI: 10.1002/adtp.202200115

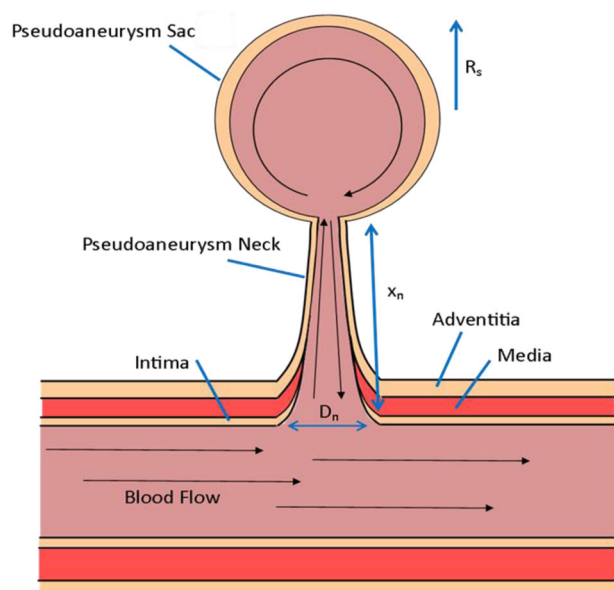


Figure 1. Schematic of a femoral artery pseudoaneurysm (PSA).

the product is wasted (fibrinogen) which increases the cost of treatment.^[2]

Before treatment of a PSA, it is diagnosed by visualizing the hyperechoic sac near the originating artery under B-mode ultrasound imaging. Then, confirmation of a PSA neck through which blood is freely flowing between the artery and the sac is performed by ultrasound color duplex imaging. The anatomy of the PSA (neck length and width and sac diameter) is measured, which is critical in determining the appropriateness of UGTI or open surgery.^[5f,g] There are no specific international guidelines available to determine if a patient is a candidate for UGTI; it is left to the surgeon's discretion, accounting for the PSA anatomy and flow dynamics.

The procedure for UGTI involves inserting a 22G needle into the PSA sac under US guidance and visualising the needle tip to be at the point furthest away from the neck. Thrombin (500 IU mL⁻¹) is slowly injected for 10 seconds, and clotting can be simultaneously visualised to validate perfusion cessation. Multiple injections of thrombin can be administered in different locations of the sac if flow persists. After the procedure, peripheral arterial pulses are taken to detect thromboembolisms in the leg together with Doppler sonography of the artery.

The most prevalent and serious complication of UGTI (reported as ≈4% of patients) is the leakage of thrombin into the main artery resulting in intra-arterial thrombosis.^[5b,f] The treatment course is typically intra-arterial infusion of tissue plasminogen activator supplemented with intravenous heparin until posterior tibial pulse is restored. In more serious cases, exploratory surgery and thrombectomy are required.^[5f,13] Many patients are not eligible for UGTI due to the high risk of thrombin escape into the main vessel. The key determinant is a short neck (<4 mm) and large sac (> 20 mm) which allows easy passage of thrombin into the artery.^[5f,g] A large sac is at high risk of rupture and it may be difficult to coagulate a large volume of blood with the limited thrombin that is injected. As more patients undergo inter-

ventional procedures that require femoral artery catheterization, there is a growing clinical need for a new treatment method that prevents thrombin leakage.

The aim of this study was to investigate the feasibility of using magnetic targeting as a means of meeting this need, specifically thrombin-loaded magnetic microbubbles (TMMB). Phospholipid-coated microbubbles are already clinical approved as ultrasound contrast agents and previous work has shown that the microbubble coating can be used as a platform to attach a desired ligand or drug molecule directly to the bubble.^[7] In addition, magnetic nanoparticles can be incorporated into the microbubble coating, enabling them to be concentrated at a target site using an externally applied magnetic field.^[8] Previous studies have demonstrated their utility for the delivery of oligonucleotides,^[9] small molecule chemotherapy drugs^[10] and thrombolytic agents.^[11] Two advantages of using microbubbles compared with, e.g., magnetic beads, are that they can be imaged using ultrasound and dissolve rapidly following treatment. By designing appropriate magnetic arrays, magnetic microbubbles can be concentrated at depths up to 7 cm depending on the blood flow conditions in the target volume.^[12]

As described in the next section, free thrombin was chemically modified with biotin to enable its attachment onto a magnetic microbubble via a biotin-avidin bridge while maintaining its enzymatic activity. Both the biotinylated thrombin and functionalized iron oxide nanoparticles were then loaded onto phospholipid-coated microbubbles and the characteristics of the bubbles (size distribution, morphology and drug loading) determined. Tissue mimicking phantoms of PSAs having a range of geometries (neck length and width and sac diameter) were produced via 3D printing and perfused with either saline or whole (equine) blood at a femoral artery flow rate (250 mL min⁻¹). A custom-built magnetic array was used to trap the bubbles in the PSA model sac and targeting efficiency determined via ultrasound imaging of the microbubbles and chromatographic analysis of the concentration of thrombin escaping from the sac.

2. Experimental Section

2.1. Materials

The composition of the microbubbles was based upon formulations that have been widely used in vitro and in vivo and are similar to those already in clinical use (e.g., Definity). A biotin end-capped PEGylated phospholipid was included both to increase the stability of the microbubbles in solution and in blood and to provide binding sites for the magnetic nanoparticle coating. Given its simplicity and the fact that several studies have shown the feasibility and safety of using avidin-biotin systems clinically^[13] an avidin-biotin conjugation strategy was chosen for the purposes of this study.

1,2-Dibehenoyl-sn-glycero-3-phosphocholine (DBPC) and 1,2-distearoyl-sn-glycero-3-phosphoethanolamine-N-[biotinyl(polyethylene glycol)-2000] were obtained from Avanti Polar Lipids (Alabaster, AL). Neutravidin protein and Alexa Fluor 594 NHS ester were purchased from Thermo Fisher Scientific (Rockford, IL). Bovine thrombin was purchased from MP Biomedicals (Solon, OH). Decafluorobutane gas was bought from FluoroMed (Round Rock, TX). Carboxymethyl

dextran-coated superparamagnetic nanoparticles (fluidMAG-CMX, 50 nm hydrodynamic diameter) were bought from Chemically GmbH (Berlin, DE). Heterobifunctional PEG (Biotin PEG succinimidyl ester, molecular weight 2000) was bought from Creative PEGWorks (Chapel Hill, NC). Inorganic salts, buffers, organic solvents, 4'-hydroxyazobenzene-2-carboxylic acid (HABA), N-biotin-tetra(ethylene glycol)-diamine trifluoroacetate (biotin-TEG-NH₂), fluorogenic thrombin substrate Boc-Val-Pro-Arg-AFC, and agar were purchased from Sigma Aldrich (St. Louis, MO). The silicone elastomer, Sylgard 184, was purchased from Farnell (Leeds, UK). Whole horse blood that was either defibrinated or mixed with the anticoagulant acid-citrate-dextrose was purchased from TCS Biosciences (Buckingham, UK).

2.2. Methods

2.2.1. Thrombin Biotinylation

Stock thrombin solution was made in 100×10^{-3} M phosphate buffer with 150×10^{-3} M NaCl at either pH 6.1, 6.5, and 7.0 to a final activity of 3000 AU mL⁻¹. The activity of thrombin reported throughout this study is referenced to the National Institutes of Health standard unit. Biotin-PEG-NHS was dissolved in the same buffer and immediately mixed with the stock thrombin solution to a final concentration of 0.6×10^{-3} M. The reaction was carried out at room temperature for 24 h. Modified thrombin was purified by four wash cycles with 0.5 mL buffer in a 10 kDa Amicon Ultra centrifugal filter.

2.2.2. Fluorescent Labeling of Thrombin

Thrombin was fluorescently labeled only for the PSA elution experiments in saline. After biotinylating thrombin, the buffer was exchanged with 100×10^{-3} M phosphate buffer at pH 8.0 in a 10 kDa Amicon Ultra centrifugal filter and 15 μ L of a freshly prepared solution of Alexa Fluor 594 NHS ester (5 mg mL⁻¹ in DMSO) were added. The reaction was carried out at room temperature for 1 h with shaking. Unreacted dye was removed by five wash cycles with 0.5 mL PBS in a 10 kDa Amicon Ultra centrifugal filter.

2.2.3. Determination of Thrombin Biotinylation

The extent of biotinylation was quantified by high-performance liquid chromatography on an Agilent 1260 Infinity II (Agilent, California, USA) with UV detection at 280 nm using a BioResolve RP mAb Polyphenyl column (450 Å, 2.7 μ m, 2.1 mm \times 100 mm; Waters, Milford, MA). The mobile phase was 0.1% trifluoroacetic acid in water (A) and 0.1% trifluoroacetic acid in acetonitrile (B). Thrombin was separated with a linear gradient of B (25%–90%) over 35 min at a flow rate of 0.8 mL min⁻¹, a temperature of 60 °C and an injection volume of 5 μ L.

2.2.4. Determination of Thrombin Activity

The activity of thrombin after modification was measured using a Boc-Val-Pro-Arg-AFC fluorogenic substrate. The assay was cal-

ibrated with a thrombin standard (Sigma Aldrich) in the concentration range of 1.6–0.05 AU mL⁻¹. In a 96-well plate, 90 μ L of a 0.22×10^{-3} M solution of substrate in DMSO were added to 10 μ L of sample. Fluorescence ($\lambda_{exc}/\lambda_{em}$ 370/450 nm) was measured immediately after addition and every 30 min for 2 h in a FLUOStar Omega plate reader (BMG Labtech, UK). The plate was sealed and kept at 37 °C between measurement. All standards and sample measurements were done in triplicate.

2.2.5. Determination of Biotin-to-Thrombin Ratio

The molar ratio of biotin to thrombin was quantified with a 4'-hydroxyazobenzene-2-carboxylic acid (HABA) displacement assay. HABA was dissolved in ultrapure water to a concentration of 2.5 mg mL⁻¹ and mixed with 10 mg of avidin to form a HABA/avidin complex. Then 180 μ L of the solution was placed into wells of a 96-well plate and the absorbance was measured at 500 nm. Next, 20 μ L of a biotinylated thrombin sample were added to each well and the absorbance was measured again at 500 nm. The molar concentration of biotin was calculated as the absorbance difference divided by 34 000 times the optical path length, according to the manufacturer's instructions.

2.2.6. Preparation of Thrombin-Loaded Magnetic Microbubbles

Iron oxide nanoparticles were biotinylated by DMTMM coupling of carboxylates on the nanoparticle coating with biotin-TEG-NH₂ as described by Beguin et al.^[14] All lipid suspensions were prepared at a 9:1 molar ratio of DBPC:DSPE-PEG₂₀₀₀-biotin and a final lipid concentration of 5 mg mL⁻¹ in PBS with 15% propylene glycol. Lipid suspensions were heated to 85 °C for 1 h under constant stirring. 4 mL of lipid suspension in an 8-mL glass vial (17 mm \times 61 mm) were then probe sonicated at low power for 2 min (QSonica Q125, 20 kHz, 3 mm probe tip, amplitude: 20%, 30 s intervals) with the tip submerged. The tip was then moved to the air water interface and the headspace flushed with PFB gas for 10 s before sonicating the suspension at 90% power for 15 s. The glass vial was then immediately removed and placed on ice for 10 min. To wash off excess lipids, bubbles were centrifuged at 350 RCF for 5 min in a 5 mL syringe. After each cycle, the supernatant was discarded and the supernatant was resuspended to 5 mL at 4 °C. The process was repeated three times for each wash cycle. At the end of the last wash, the microbubbles were resuspended in 2 mL of a 0.5 mg mL⁻¹ neutravidin solution and incubated for 10 min at 4 °C. Unbound avidin was removed by three wash cycles of centrifugation as described above, and the microbubbles supernatant was then resuspended in 2 mL of a 25 mg mL⁻¹ solution of biotinylated nanoparticles and incubated for 10 min at 4 °C. Unbound nanoparticles were removed by a single cycle of centrifugation, and the microbubbles supernatant was mixed with 2 mL of neutravidin solution (0.5 mg mL⁻¹) and incubated for 10 min at 4 °C. Unbound neutravidin was removed by centrifugation and the microbubbles supernatant was then resuspended in PBS. Before loading the magnetic microbubbles with thrombin, the size distribution and concentration were measured with a Coulter counter (Multisizer 4e, Beckman Coulter, Indianapolis, IN) using a 2 μ L microbubble sample in 10 mL of

Table 1. Pseudoaneurysm phantom dimensions.

Structure	Sac diameter A [mm]	Neck length B [mm]	Neck diameter C [mm]
1	25	8	4
2	25	4	4
3	35	4	6
4	35	4	8
5	50	4	6

Isoton. Thrombin was loaded on to the bubbles by diluting bubbles to 10^8 bubbles mL^{-1} , mixing with biotinylated thrombin to a final concentration of 100 AU mL^{-1} and incubating for 10 min on ice under gentle mixing. One wash cycle was performed to remove unbound thrombin. The loading was performed immediately prior to each experiment.

2.2.7. Transmission Electron Microscopy of Microbubbles

1 μL of sample was applied to a freshly glow discharged carbon-coated 300 mesh copper grid held in self-closing forceps, gently blotted and left to air dry. The samples were then stained with 20 μL of 2% uranyl acetate for 10 s, blotted and air-dried. Grids were imaged at 120 kV in a ThermoFisher Tecnai 12 TEM using a Gatan OnceView camera.

2.2.8. Thrombin-Loaded Magnetic Microbubble Retention

Magnetic retention experiments were performed in an agar phantom consisting of a $15 \text{ cm} \times 15 \text{ cm} \times 1 \text{ cm}$ block containing a 1.6 mm diameter channel through which bubbles were perfused at 0.5 mL min^{-1} using a syringe pump. A custom-built magnet consisting of five concentrically stacked permanent magnetic disks of decreasing diameter housed in an aluminum bracket was positioned 3 or 5 cm below the center of the agar channel (for details see ref. [15]). Microbubbles were visualized using a Philips iU22 clinical scanner operating at an MI of 0.04. Image analysis was performed over 25 frames by calculating the average pixel intensity within the region of interest (ROI) with and without the magnet and compared against the background measurement.

2.2.9. Microbubble Capture in Pseudoaneurysm

A polydimethylsiloxane (PDMS) flow phantom was constructed with an embedded PSA geometry with 10:1 ratio of prepolymer to curing agent. The mixture was degassed until all bubbles were removed and then placed in a 70°C oven for 3 h. The embedded PA geometry was removed by cutting the phantom in half with a scalpel and gluing the phantom back together with an epoxy adhesive to create a leak-free seal. The three main features of a PA are the neck length, neck diameter, and sac diameter. Five different combinations were investigated as shown in **Table 1**. The main vessel size was 0.8 cm which is approximately the same diameter as the common femoral artery in adult humans. PDMS

was chosen as having both optical and acoustic transparency to enable visualization of the clotting process. A 1 mL syringe was filled with either thrombin loaded microbubbles or thrombin alone and placed in a syringe pump that was connected by a 24 G needle inserted at the top of the PSA cavity (the furthest point from the PSA neck). The flow rate of the main vessel was set to 250 mL min^{-1} and the flow was allowed to equilibrate for 2 min. The magnet was fastened in place by a cutout in the phantom holder to ensure reproducible placement of the magnet between experiments. The experiment started when the syringe pump was turned on at a flow rate of 2.4 mL min^{-1} to dispense a volume of 1 mL. Samples were taken periodically from a port downstream of the PSA sac and collected in 1 mL syringes. The total experimental time was 9 min. Samples were then taken to measure the amount of thrombin that had leaked from the sac by fluorescence detection ($\lambda_{\text{exc}}/\lambda_{\text{em}}$ 590/610 nm) on a FLUOStar Omega (BMG Labtech, UK) or by direct injection into a 1260 Infinity II Fluorescence Detector (Agilent, California, USA).

2.2.10. Determination of Thrombin Elution from Pseudoaneurysm Cavity in Saline

For experiments in saline and in samples that may have contained thrombin-loaded magnetic microbubbles, the syringes were sealed and repeatedly pressurized firmly by hand for 1 min to destroy any bubbles. Samples were used as collected for thrombin-only experiments. Fluorescence was measured as described above.

2.2.11. Determination of Thrombin Elution from Pseudoaneurysm Cavity in Whole Blood

For experiments in horse blood and in samples that may have contained thrombin-loaded magnetic microbubbles, the collection syringes were sealed and repeatedly pressurized firmly by hand for 1 min to destroy any bubbles. Samples were used as collected for thrombin only experiments. Then the blood was placed in 1.5 mL Eppendorf tubes and centrifuged at 1000 RCF for 5 min to separate plasma. Then, 100 μL of plasma was carefully pipetted into streptavidin-coated wells (Pierce Streptavidin Coated High-Capacity Plates; ThermoFisher), and left to incubate for 2 h at room temperature to bind any biotinylated thrombin. The wells were then washed with wash buffer ($25 \times 10^{-3} \text{ M}$ Tris-buffered saline pH 7.2, 0.1% BSA, 0.05% Tween) and 100 μL of a $15 \times 10^{-6} \text{ M}$ solution of Boc-Val-Pro-Arg-AFC thrombin fluorogenic substrate were added. After 2 h of incubation at 37°C , fluorescence ($\lambda_{\text{exc}}/\lambda_{\text{em}}$ 370/450 nm) was measured by direct injection into a 1260 Infinity II Fluorescence Detector (Agilent, California, USA).

2.3. Statistical Analysis

For all the statistical analyses, statistical packages in OriginLabs (Origin(Pro), 2021b (9.85), OriginLab Corporation, Northampton, MA) were used. For **Figure 3C**, to determine the significant difference between the Reaction curves and Control curves, a

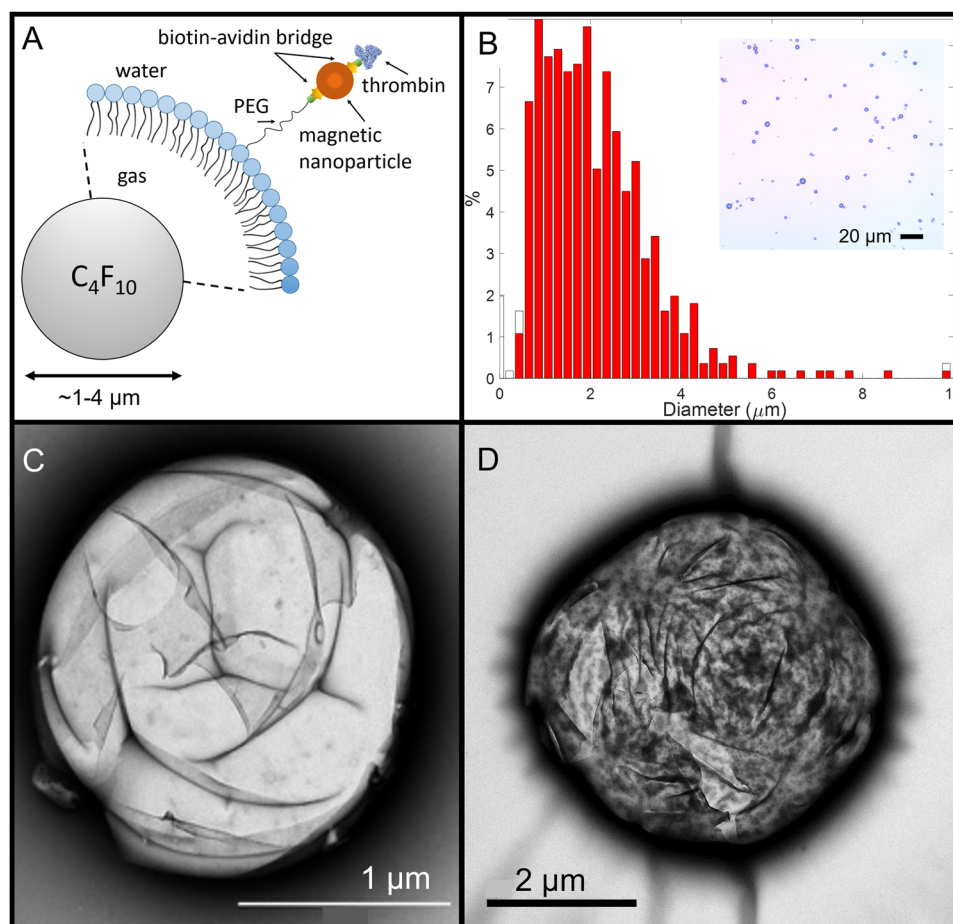


Figure 2. A) Illustration of the thrombin-loaded magnetic microbubbles (TMMB) construct. B) Typical size distribution of the TMMB (inset shows an optical microscopy image of TMMB in suspension). C) Transmission electron microscopy image of microbubble with no magnetic nanoparticles. D) Transmission electron microscopy image of TMMB.

Kolmogorov–Smirnov (KS) test was used (the associated *p*-values were < 0.05). For **Figure 4B,C**, a one-way analysis of variance test with post hoc Tukey's method was used to determine the significance of the difference between the means for the three samples (Clean MB, MM, and TMM). For **Figure 5**, a KS test was used for each set of geometries (the associated *p*-values were < 0.05).

3. Results and Discussion

3.1. Microbubble Characterization

The shell of thrombin-loaded magnetic microbubbles comprised two phospholipid species with the secondary lipid component (10%) enabling the binding of the magnetic nanoparticle to the outside part of the shell via a biotin avidin bridge. Thrombin was then conjugated to the nanoparticle after binding neutravidin to the remaining available binding sites. Thrombin at the outermost part of the bubble allowed for the protease to easily interact with the target protein (fibrinogen) and the overall bubble construct is illustrated in **Figure 2A**. The filling gas used for the bubbles was perfluorobutane that yielded bubble size distributions shown in **Figure 2B** and concentrations of $10^9 \text{ mL}^{-1} \pm 3 \times 10^7$. Magnetic

nanoparticle attachment was confirmed by the strong response of the microbubbles to a magnetic field gradient in a flow phantom (**Figure 4**) and corroborated by comparing transmission electron microscopy images of microbubbles with and without magnetic nanoparticles (**Figure 2C,D**).

3.2. Drug Loading

The biotin–avidin conjugation scheme that was used required biotinylation of thrombin. N-hydroxysuccinimide (NHS) esters can react with surface exposed primary amino groups on lysine residues and at the N terminus. The pH of the reaction can affect both selectivity, with N-terminal conjugation favored at pH < 7,^[16] and biotinylation yield, which increases with pH and typically exhibits a maximum around pH 8.^[17] While high selectivity is desirable in order to minimize loss of activity, carrying out the reaction at low pH can result in incomplete biotinylation and, as a consequence, decreased thrombin loading on TMMB. In order to maximize the activity of TMMB, the activity of biotinylated thrombin and the degree of biotinylation must be simultaneously optimized. To this end, we measured activity and fraction of

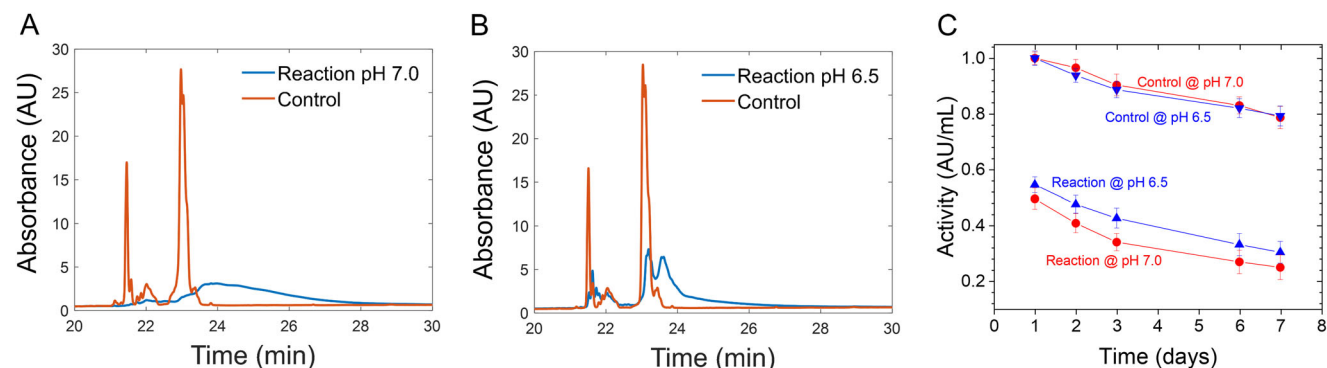


Figure 3. A,B) High-performance liquid chromatography of unmodified thrombin (orange) and biotinylated thrombin (blue) at pH 7.0 and pH 6.5, respectively. C) The activity of unmodified thrombin and biotinylated thrombin over 7 d at pH 7.0 (red) and pH 6.5 (blue). Results are the mean average of three samples. Error bars indicate one standard deviation. A Kolmogorov–Smirnov test was used to compare the reaction curves and control curves. The associated *p*-values were <0.05 .

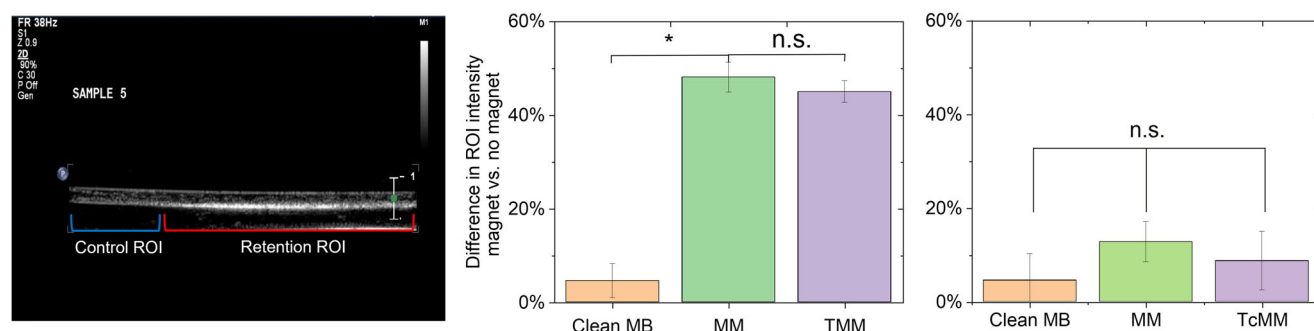


Figure 4. A) Example of B-mode ultrasound frame showing the regions analyzed to determine retention of thrombin-loaded magnetic microbubbles (TMMB) 1 min after bolus injection during continuous flow in a 1.6 mm agar channel. The difference in magnetic retention for three microbubble samples: clean MB, magnetic microbubbles (MM), and TMMB at a B) 3-cm distance and C) 5-cm distance from magnet face to the center of the channel. Results are the mean average of three samples. Error bars indicate one standard deviation. A one-way analysis of variance test with post hoc Tukey method was used to determine the significance of the difference between the means for the three samples (* indicates $p < 0.05$, n.s. = not significant).

unmodified thrombin in batches of thrombin biotinylated under different pH conditions. High-performance liquid chromatography showed that $86 \pm 4\%$ of the thrombin was biotinylated when the reaction was carried out at pH 7 (Figure 3A) compared to $65 \pm 6\%$ at pH 6.5 (Figure 3B), with only a negligible difference in activity (Figure 3C). The reaction at pH 7 was therefore used for the rest of the study.

3.3. Magnetic Response

Magnetic actuation of the TMMB was first investigated in a straight channel in flow (0.2 mL min^{-1}) with a custom-built magnetic array. Approximately 2×10^7 TMMB were injected over the course of 1 min. The agar channel was elevated above the magnet face by either 3 or 5 cm, to delimit the magnetic field strength necessary to trap bubbles against the wall based on the results of our previous study.^[15] A typical B-mode image after 1 min of flow is shown in Figure 4A and there is a clear hyperechoic layer in the region of interest directly above the magnetic array at a separation distance of 3 cm. Figure 4B shows significant bubble retention for both unloaded magnetic microbubbles ($48 \pm 3\%$) and the thrombin-loaded magnetic microbubble ($42 \pm 2\%$) compared to

a microbubble with no magnetic material ($4 \pm 3\%$, clean MB). At the 5 cm separation distance (Figure 4C), the retention is reduced to $15 \pm 4\%$ for the unloaded magnetic microbubbles and $10 \pm 3\%$ for the thrombin-loaded magnetic microbubbles and there is no statistically significant difference to microbubbles with no magnetic material.

3.4. Thrombin Retention in a Tissue-Mimicking Phantom

To establish that TMMB can reduce thrombin escape when coupled with a magnet compared to the current treatment method of direct thrombin injection, a PDMS flow phantom embedded with five different PSA anatomies were built (Table 1). Figure 5A–E showed that in all cases TMMB coupled with the magnet reduced the escape of thrombin over a 7-min period. PSA structure in Figure 5D (structure 3) showed the least amount of thrombin leaked out of the PA sac with a maximum of $0.08 \pm 0.01 \text{ AU mL}^{-1}$ at the end of the experiment compared to the free thrombin injection maximum of $0.48 \pm 0.02 \text{ AU mL}^{-1}$. The PSA structure 2 showed the greatest reduction of thrombin escape compared to the freely injected thrombin. Interestingly, Figure 5C shows a drop in thrombin concentration from first to second timepoint

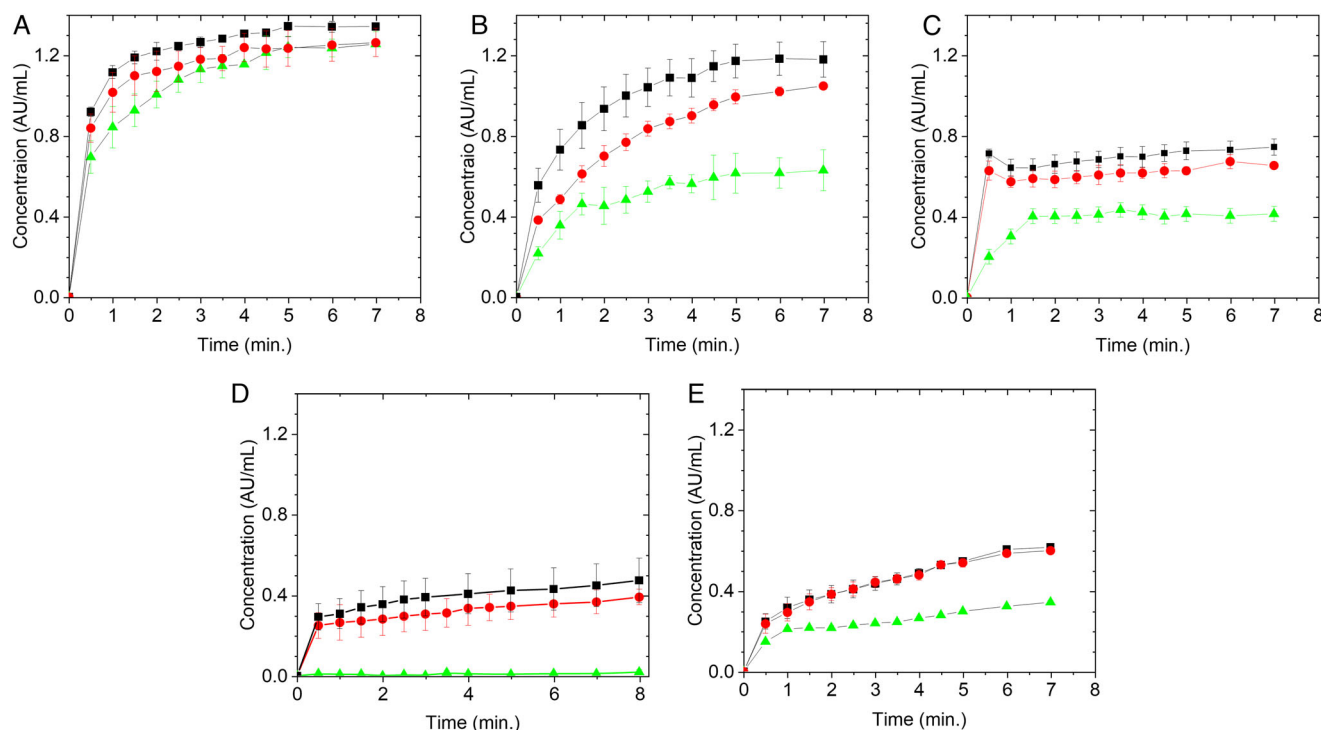


Figure 5. Thrombin-loaded magnetic microbubble (TMMB) retention in pseudoaneurysms using five different geometries. The three thrombin concentration curves correspond to injection of free thrombin with the magnet present (black squares), TMMB with no magnet present (red circles), and TTM with the magnet present (green triangles). A) cavity diameter = 25 mm, neck diameter = 6 mm, neck length = 4 mm. B) cavity diameter = 25 mm, neck diameter = 6 mm, neck length = 8 mm. C) cavity diameter = 35 mm, neck diameter = 8 mm, neck length = 4 mm. D) cavity diameter = 35 mm, neck diameter = 6 mm, neck length = 4 mm. E) cavity diameter = 50 mm, neck diameter = 6 mm, neck length = 4 mm. Results are the mean average of three samples. Error bars indicate one standard deviation. A Kolmogorov–Smirnov test was used for each set of geometries (the associated *p*-values were <0.05).

for freely injected thrombin and TMMB with no magnet. This behavior is due to the neck structure being both wide (8 mm) and short (4 mm) thus allowing easy passage of thrombin from the sac into the main vessel. The drop in measured concentration at the second timepoint is due to the time required (30 s) to dilute the initial burst of thrombin into the main vessel. The subsequent timepoints then rise as more thrombin diffuses into the sac and no clotting could occur in the saline-only experiments. It has been shown in previous work that, owing to the size of MBs, red blood cells may interfere with their capture by obstructing the path of the bubbles towards the magnet.^[18] **Figure 6A** shows that the amount of thrombin exiting the pseudoaneurysm cavity and entering the main vessel was 3.5 times greater for freely injected thrombin compared to TMMB. Therefore, the blood components, especially red blood cells, did not significantly prevent the capture of TMMB in this study. The size and geometry of the phantoms in the two studies are quite different and this is likely to be the reason for the difference in the influence of red blood cells. In the previous study, the aim was to direct bubbles to the wall of a narrow vessel (200 μ m inner diameter) under laminar flow conditions. In this case the red blood cells physically impeded the movement of the bubbles to the wall so that a much smaller number was able to make contact with it before being washed out of the vessel. In the present study, however, the volume of the PSA phantom sac was much larger and the fluid flow patterns much more complex, enabling bubbles more freedom to travel toward

the magnet. In addition, the interaction between bubbles and red blood cells would be beneficial to promote clotting.

3.5. Limitations and Future Work

Concerns have been raised as to the immunogenicity of avidin in humans as there are naturally occurring human anti-avidin antibodies (HAVA), the levels of which become elevated after exposure to avidin in both human and mouse models. However, Petronzelli et al. showed that avidin exposure did not actually cause any adverse clinical symptoms, suggesting that its use may be acceptable in humans.^[13d] It is also important to note that systemic exposure to either avidin or biotin in this case would be very limited. If necessary, however, it would be possible to substitute an alternative coupling mechanism for the thrombin and magnetic particles, e.g., maleimide–thiol Michael addition or strain-promoted [3+2] azide–alkyne cycloaddition.^[17,19]

The absolute amount of thrombin on microbubbles was not directly measured. While the thrombin dose could potentially be inferred from the amount of thrombin that was not bound to the bubbles, this likely would not be acceptable for clinical translation of the microbubble formulation and an alternative quantification method would be required; although ultimately it is the activity of the attached thrombin that is the most clinically relevant parameter.

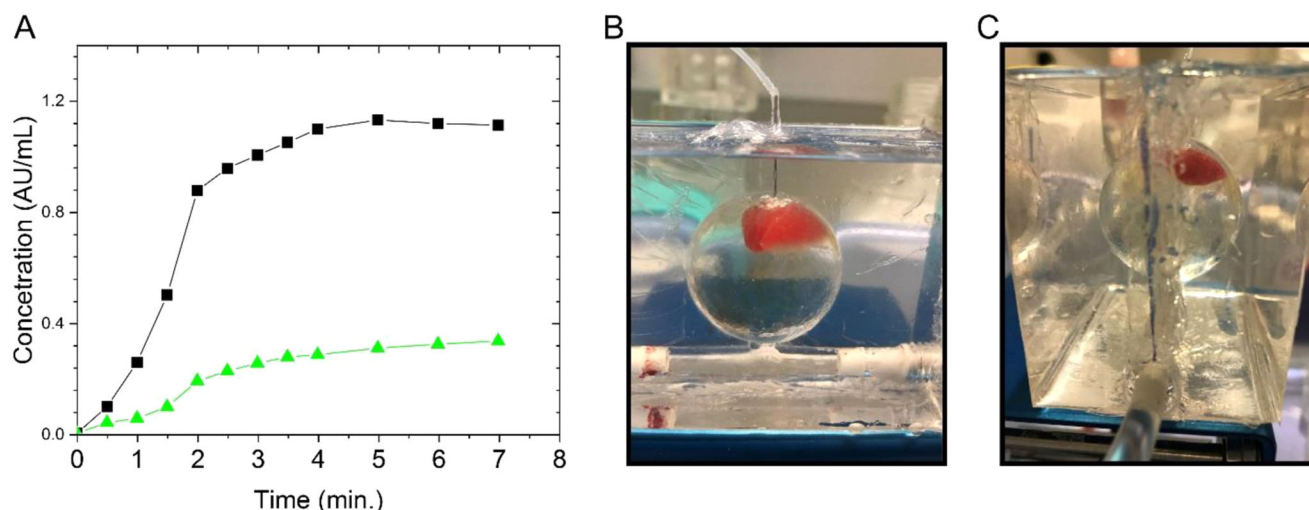


Figure 6. A) Thrombin-loaded magnetic microbubble retention in a pseudoaneurysm using defibrinated horse blood. The two concentration curves (black squares—free thrombin injection and green triangles—TMMB) represent the amount of thrombin leaving the pseudoaneurysm cavity and entering the main vessel (single measurement). B) Picture of a typical clot that forms after injection of TMMB and with the magnet in position using recalcified citrated whole horse blood and C) from a different angle the clot preferentially forms nearer to the side that the magnet is placed. The cavity and neck dimensions were cavity diameter = 35 mm, neck diameter = 8 mm, neck length = 4 mm.

TMMB stability was not evaluated directly in this study because this is a less important consideration for the PSA treatment than for the conventional use of microbubbles as contrast agents. For PSA treatment, TMMB administration would always be directly into the PSA with the aim of very rapidly forming a clot (as demonstrated in Figure 6). Thus, the TMMB would only need to be stable for a short period of time once removed from the vial. A long-term stability study of TMMB under storage conditions would need to be completed for future translation, but was outside the scope of the present study.

The magnetic array could be improved to generate a stronger magnetic force and hence more efficient capture of the bubbles at greater tissue depths. For convenience, off-the-shelf permanent magnets were used in this study, but higher quality neodymium magnets would increase the magnetization of the array and hence the force it could produce.^[20] Protocols for the safe use of the magnet in a clinical setting would then need to be developed.^[21]

The mechanical properties of PDMS do not mimic those of soft tissues and the shape of the PA phantom in this study was highly idealized. For example, the neck of the PA is not necessarily orthogonal to the main femoral artery and the sac may be highly asymmetric. These factors may alter the flow profile in the PA cavity and thus influence the feasibility of confining magnetic microbubbles. Further simulations (computational and physical) are required to explore a wider range of PSA profiles, although the models used here would in fact be expected to represent the most challenging geometries for bubble confinement.

4. Conclusion

This study investigated the feasibility of using magnetic microbubbles as a means of improving retention of thrombin in a PSA under ultrasound-guided injection. Thrombin-loaded magnetic microbubbles were successfully formulated and the activ-

ity of the bound thrombin confirmed. Successful retention of magnetic microbubbles in a tissue-mimicking phantom of a PSA was achieved for a range of different geometries (sac diameter, neck diameter, and neck length) with substantial improvements over free thrombin injection in the majority of cases. Clotting of whole (equine) blood was also confirmed in the phantom. By reducing the risk of downstream thrombosis it is hoped that the range of PSA geometries amenable to treatment by thrombin injection could be substantially increased with corresponding improvements in patient experience and safety.

Acknowledgements

The authors gratefully acknowledge Heart Research UK for funding this study; Dr. Errin Johnson of the Dunn School Bioimaging Facility for her kind assistance with the electron microscopy; Mr. Peter Walters of the 3D printing hub in the Department of Engineering Science; and Mr. Jim Fisk of the Biomedical Engineering workshop for assistance with construction of the experimental rigs.

Conflict of Interest

A.H., R.L. and E.S. have filed a patent on a method for the minimal invasive treatment of pseudoaneurysms using magnetic microbubbles. All other authors declare no conflict of interest.

Data Availability Statement

The data that support the findings of this study are available from the corresponding author upon reasonable request.

Keywords

drug delivery, magnetic targeting, microbubbles, pseudoaneurysm, thrombin, ultrasound guided

Received: June 20, 2022
Revised: August 19, 2022
Published online: September 16, 2022

- [1] M. Stolt, R. Braun-Dullaes, J. Herold, *Vasa Suppl.* **2018**, 47, 177.
- [2] N. Kontopodis, C. V. Ioannou, *Eur. J. Vasc. Endovasc. Surg.* **2015**, 50, 721.
- [3] a) B. Toursarkissian, B. T. Allen, D. Petrinc, R. W. Thompson, B. G. Rubin, J. M. Reilly, C. B. Anderson, M. W. Flye, G. A. Sicard, *J. Vasc. Surg.* **1997**, 25, 803; b) R. Morgan, A. M. Belli, *J. Vasc. Interv. Radiol.* **2003**, 14, 697.
- [4] C. Cope, R. Zeit, *AJR, Am. J. Roentgenol.* **1986**, 147, 383.
- [5] a) N. J. Shatnawi, N. A. Al-Zoubi, J. Jarrah, Y. Khader, M. Heis, M. H. Al-Omari, *SAGE Open Med.* **2019**, 7, 205031211984370; b) P. A. Stone, M. Martinez, S. N. Thompson, D. Masinter, J. E. Campbell, J. R. Campbell II, A. F. AbuRahma, *Ann. Vasc. Surg.* **2016**, 30, 45; c) P. A. Stone, S. N. Thompson, B. Hanson, D. Masinter, *Vasc. Endovasc. Surg.* **2016**, 50, 217; d) E. Di Cera, *Mol. Aspects Med.* **2008**, 29, 203; e) R. I. Litvinov, J. W. Weisel, *Matrix Biol.* **2017**, 60, 110; f) F. Ahmad, S. A. Turner, P. Torrie, M. Gibson, *Clin. Radiol.* **2008**, 63, 1310; g) E. Y. Yang, M. M. Tabbara, P. G. Sanchez, A. M. Abi-Chaker, J. Patel, A. Bornak, K. M. Jones, J. Rey, *Ann. Vasc. Surg.* **2018**, 47, 121.
- [6] T. Yoo, J. E. Starr, M. R. Go, P. S. Vaccaro, B. Satiani, M. J. Haurani, *Vasc. Endovasc. Surg.* **2017**, 51, 368.
- [7] a) F. S. Villanueva, R. J. Jankowski, S. Klivanov, M. L. Pina, S. M. Alber, S. C. Watkins, G. H. Brandenburger, W. R. Wagner, *Circulation* **1998**, 98, 1; b) J. Liu, N. J. Agrawal, A. Calderon, P. S. Ayyaswamy, D. M. Eckmann, R. Radhakrishnan, *Biophys. J.* **2011**, 101, 319; c) A. M. Takalkar, A. L. Klivanov, J. J. Rychak, J. R. Lindner, K. Ley, *J. Controlled Release* **2004**, 96, 473; d) C. J. Slagle, D. H. Thamm, E. K. Randall, M. A. Borden, *Bioconjugate Chem.* **2018**, 29, 1534; e) S. Pochon, I. Tardy, P. Bussat, T. Bettinger, J. Brochot, M. von Wronski, L. Passantino, M. Schneider, *Invest. Radiol.* **2010**, 45, 89; f) S. Unnikrishnan, Z. M. Du, G. B. Diakova, A. L. Klivanov, *Langmuir* **2019**, 35, 10034.
- [8] a) E. Stride, C. Porter, A. G. Prieto, Q. Pankhurst, *Ultrasound Med. Biol.* **2009**, 35, 861; b) D. Vlaskou, O. Mykhaylyk, R. Giunta, I. Neshkova, N. Hellwig, F. Kroetz, C. Bergemann, C. Plank, *Mol. Ther.* **2006**, 13, S290.
- [9] D. Vlaskou, O. Mykhaylyk, C. Plank, *Methods Mol. Biol.* **2019**, 1943, 253.
- [10] Y. Sheng, E. Beguin, H. Nesbitt, S. Kamila, J. Owen, L. C. Barnsley, B. Callan, C. O'Kane, N. Nomikou, R. Hamoudi, M. A. Taylor, M. Love, P. Kelly, D. O'Rourke, E. Stride, A. P. McHale, J. F. Callan, *J. Controlled Release* **2017**, 262, 192.
- [11] a) M. de Saint Victor, L. C. Barnsley, D. Carugo, J. Owen, C. C. Cousios, E. Stride, *Ultrasound Med. Biol.* **2019**, 45, 1151; b) B. H. Zhang, O. W. Kim, H. Y. Wu, Y. Gao, X. N. Jiang, *Ultrasonics* **2019**, 98, 62.
- [12] L. C. Barnsley, D. Carugo, E. Stride, *J. Phys. D: Appl. Phys.* **2016**, 49, 225501.
- [13] a) R. De Santis, A. M. Anastasi, V. D'Alessio, A. Pelliccia, C. Albertoni, A. Rosi, B. Leoni, R. Lindstedt, F. Petronzelli, M. Dani, A. Verdoliva, A. Ippolito, N. Campanile, V. Manfredi, A. Esposito, G. Cassani, M. Chinol, G. Paganelli, P. Carminati, *Br. J. Cancer* **2003**, 88, 996; b) G. Paganelli, M. Ferrari, M. Cremonesi, C. De Cicco, V. Galimberti, A. Luini, P. Veronesi, M. Fiorenza, P. Carminati, C. Zanna, R. Orecchia, U. Veronesi, *Breast* **2007**, 16, 17; c) C. Veyrat-Follet, N. Vivier, M. Trellu, C. Dubruc, G. J. Sanderink, *J. Thromb. Haemostasis* **2009**, 7, 559; d) F. Petronzelli, A. Pelliccia, A. M. Anastasi, R. Lindstedt, S. Manganello, L. E. Ferrari, C. Albertoni, B. Leoni, A. Rosi, V. D'Alessio, K. Deiana, G. Paganelli, R. De Santis, *Cancer Biother. Radiopharm.* **2010**, 25, 563.
- [14] E. Beguin, M. D. Gray, K. A. Logan, H. Nesbitt, Y. Sheng, S. Kamila, L. C. Barnsley, L. Bau, A. P. McHale, J. F. Callan, E. Stride, *J. Controlled Release* **2020**, 317, 23.
- [15] L. C. Barnsley, M. D. Gray, E. Beguin, D. Carugo, E. Stride, *Adv. Mater.* **2018**, 3, 1800081.
- [16] C. Rosen, M. Francis, *Nat. Chem. Biol.* **2017**, 13, 697.
- [17] G. T. Hermansen, *Bioconjugate Techniques*, 2nd ed., Academic, New York, NY **2008**.
- [18] J. Owen, P. Rademeyer, D. Chung, Q. Cheng, D. Holroyd, C. Cousios, P. Friend, Q. A. Pankhurst, E. Stride, *Interface Focus* **2015**, 5, 20150001.
- [19] R. Browning, N. Thomas, L. K. Marsh, L. R. Tear, J. Owen, E. Stride, N. J. Farrer, *ChemistryOpen* **2021**, 10, 1170.
- [20] L. C. Barnsley, D. Carugo, J. Owen, E. Stride, *Phys. Med. Biol.* **2015**, 60, 8303.
- [21] X. Zhang, G. Chen, X. Fu, Y. Wang, Y. Zhao, *Adv. Mater.* **2021**, 33, 2104932.